PNAS
www.pnas.org

Supplementary Information for

The influence of iodine on the Antarctic stratospheric ozone hole

Carlos A. Cuevas[1,*], Rafael P. Fernandez[2-3], Douglas E. Kinnison[4], Qinyi Li[1], Jean-François Lamarque[5], Tarek Trabelsi[6], Joseph S. Francisco[6], Susan Solomon[7], and Alfonso Saiz-Lopez[1,*]

[1]Department of Atmospheric Chemistry and Climate, Institute of Physical Chemistry Rocasolano, CSIC, Madrid, 28006, Spain
[2]Institute for Interdisciplinary Science, National Research Council (ICB-CONICET), Mendoza, 5501, Argentina
[3]School of Natural Sciences, National University of Cuyo (FCEN-UNCuyo), Mendoza, 5501, Argentina
[4]Atmospheric Chemistry Observation and Modeling, National Center for Atmospheric Research, Boulder, CO 80305, USA
[5]Climate and Global Dynamics Laboratory, National Center for Atmospheric Research, Boulder, CO 80305, USA
[6]Department of Chemistry, University of Pennsylvania, Philadelphia, PA 19104, USA
[7]Department of Earth, Atmospheric, and Planetary Sciences, Massachusetts Institute of Technology, Cambridge, MA, 02139, USA

*Corresponding author: Alfonso Saiz-Lopez and Carlos A. Cuevas

Email: a.saiz@csic.es; ccuevas@iqfr.csic.es

This PDF file includes:

Supplementary information test

Theoretical calculations for the destruction of photo-dissociation of iodate

Two plausible mechanisms may lead to the photochemical destruction or the photodissociation of IO_3^-:

Mechanism 1

Table S1 predict the vertical excitation energies for the low-lying electronic states of IO_3^-. Absorption of a photon to these states or to the detachment continuum (hv < 263 nm ADE (1)) lead to the photodetachment. In this case, many products may be produced such as:

$$IO_3^- + hv \rightarrow IO_3 + e$$

IO_3^- photodetaches an electron to produce neutral IO_3.
Other possible products are

$$IO_3 + hv \rightarrow IO_2^- + O\ (^1D)$$
$$\rightarrow IO_2 + O^-(^2P)$$
$$\rightarrow IO_2^- + O\ (^3P)$$

Depending on the absorption energy, the above channels are plausible, since, there is high density of electronic states of the IO_3^- (for hv < 263 nm) and these states cross the ground state of the neutral which easily lead to photodetachment.

Mechanism 2

IO_3^- is characterized by many excited stable states and present real minimum in their PES (their minimum located below the ground state of the neutral and correlate to dissociation limits located below the first dissociation limit of the neutral, Fig S1). Absorption of a photon in visible or near UV region i.e. (263 < hv < 442 nm) to these states may lead to the production of IO_2^- +O. Indeed, three triplet states correlate to the first dissociation limit, and these states are crossed by singlet states that correlates to IO_2+O^- dissociation limit. In this case, the photodissociation process may occur through the spin-orbit coupling at the crossing point between singlet-triplet to produce IO_2^- and O in their ground electronic states.

Moreover, the first excited singlet state of IO_3^- is unstable relative to IO^- + O_2 dissociation limit. Since the minimum of S_1 located above the IO^- + O_2 dissociation limit and absorption to S1 state may lead to IO^- + O_2 product and this competes with the production of IO_2^- +O and IO_3 + e.
The destruction of IO_3^- easily occurs for shorter wavelength whereas its photodissociation for longer wavelength is less plausible since the lowest singlet and triplet state are weakly bounded and their minimum located below the first dissociation limits.

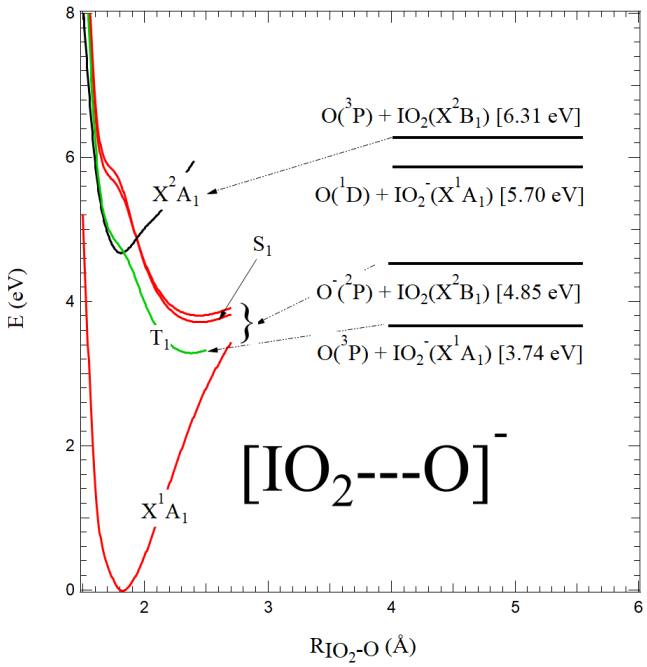

Fig S1. MRCI+Q/aug-cc-pVTZ-PP PES of the low-lying excited state of IO_3^- along the IO bond length. The electronic ground state of the neutral IO_3 is shown in black. Default active space selected for all calculations at MRCI+Q level.

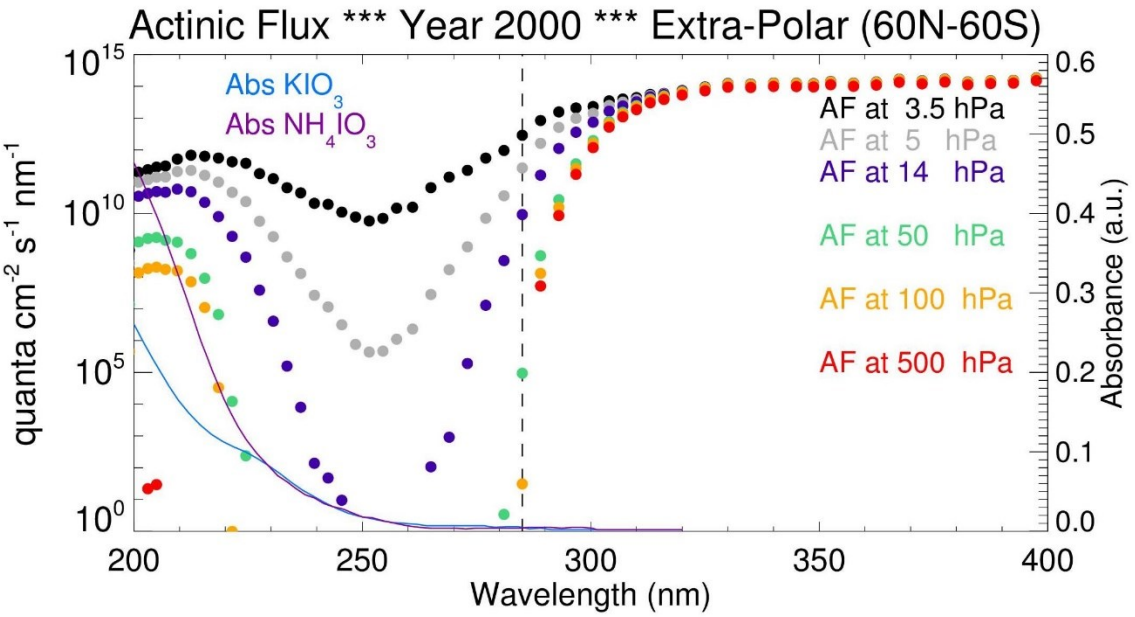

Figure S2. Modeled 2000 annual averaged wavelength dependent Actinic flux (AF) at different altitudes (colored dots, left axis), together with the absorbance of iodate (KIO_3 and NH_4IO_3) species (blue and purple lines, right axis) from Galvez et al., 2016(2).

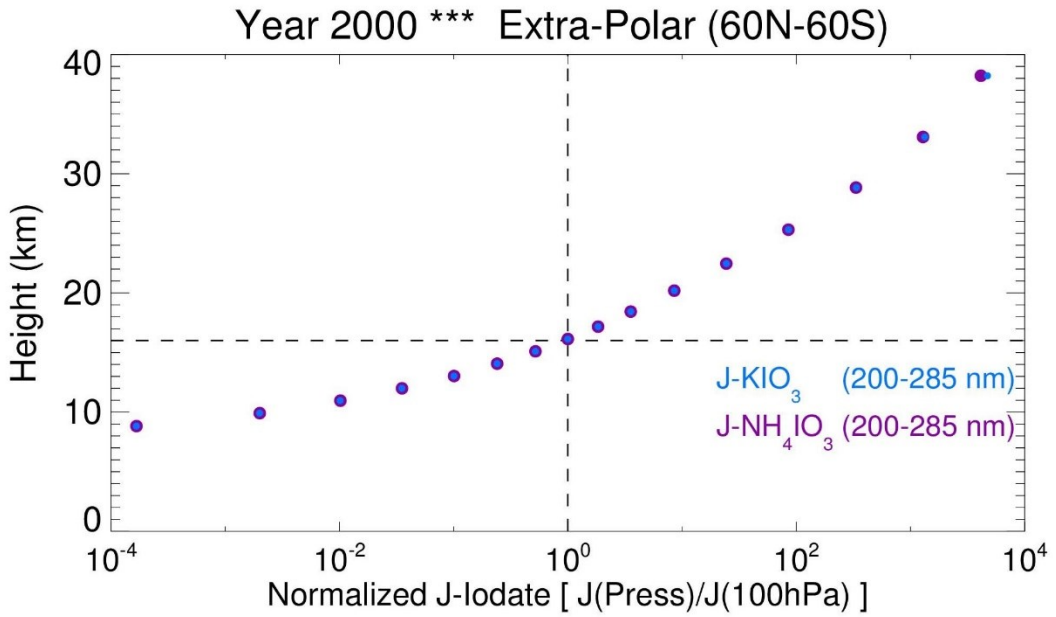

Figure S3. Vertical profile of normalized iodate (KIO_3 and NH_4IO_3) photolysis rates averaged during year 2000 within the extra-polar (60ºS-60ºN) region. J-iodate normalization has been performed with respect to the J-value obtained at approx. 100 hPa (~16-17 km). The wavelength range used for the photolysis rate computation is 200-285 nm (Fig. S2).

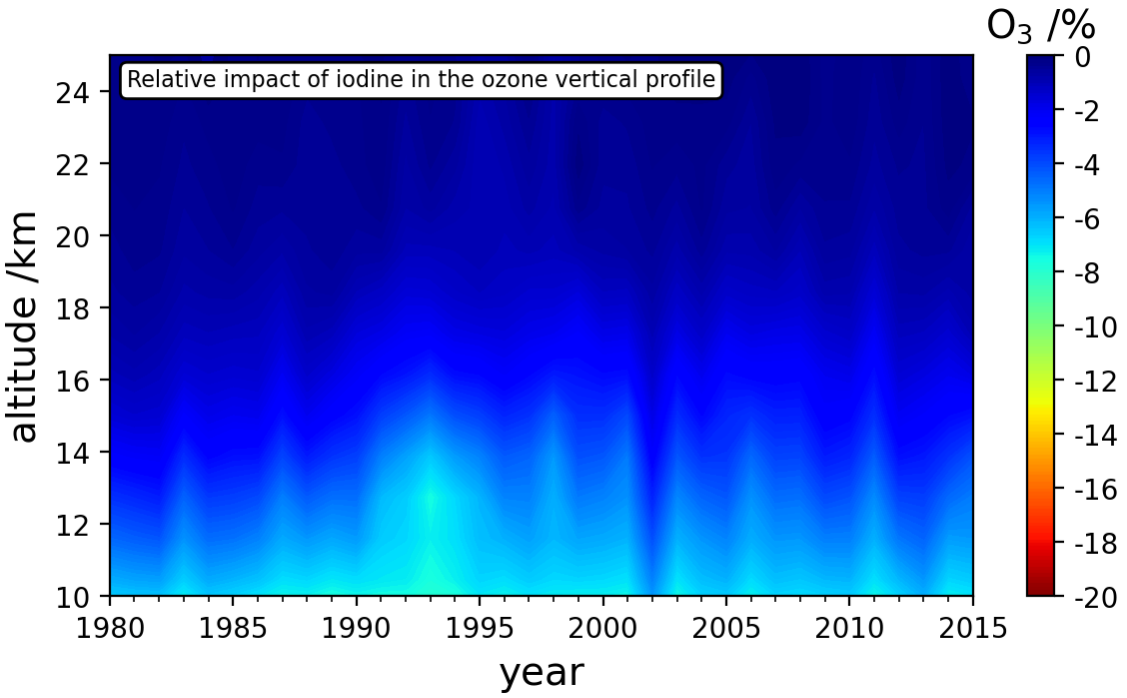

Figure S4. Impact of iodine in the ozone vertical profile, averaged in September and October in the 90ºS-70ºS region during the 1980-2015 period. Equivalent to Fig. 2a for the "I_{part}" simulation. Color scale is the same as Fig. 2a for better comparison.

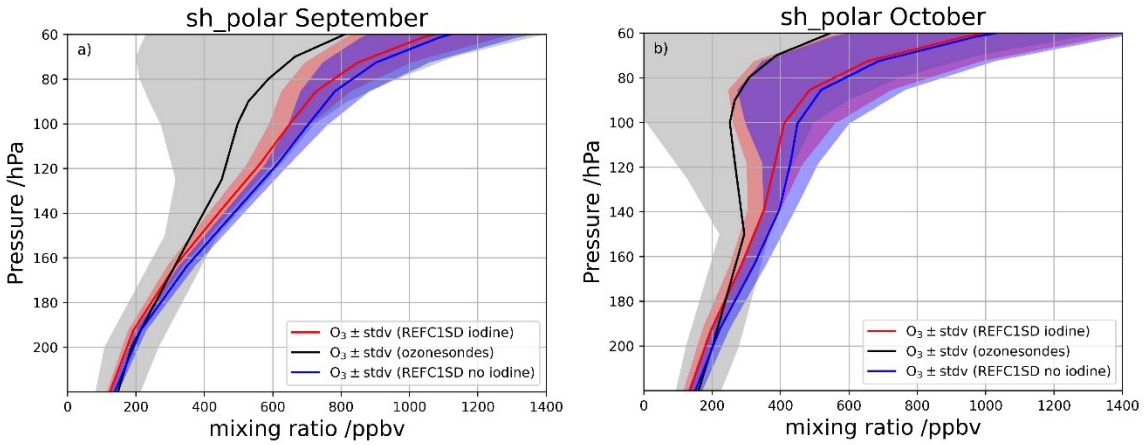

Figure S5. Comparison of model output (from base iodine and without iodine simulations) to ozonesonde climatology between 1995 and 2011 for the months of September and October. Observations from (3). Ozonesonde climatology include observation from the Marambio, Neumayer and Syowa stations. Model output is the monthly average over the three stations (Marambio: 66º-62ºS and 58º-54ºW; Neumayer: 72º-68ºS and 10º-6ºW; Syowa: 71º-67ºS and 37-41ºE)

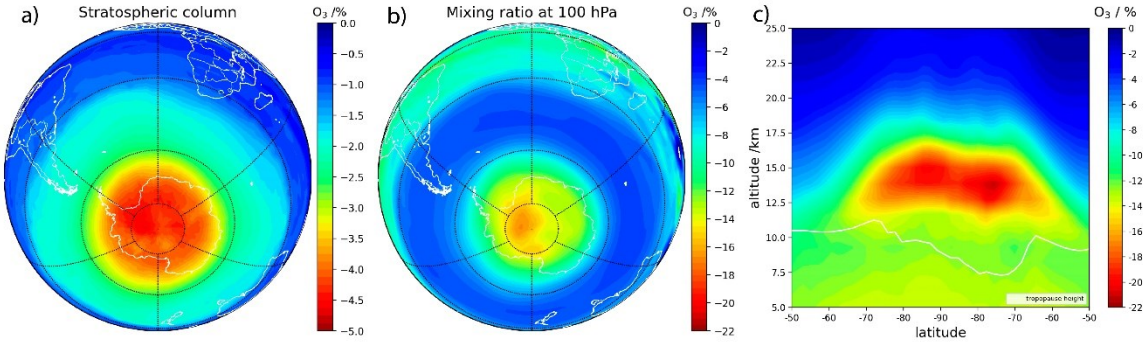

Figure S6. Effect of iodine chemistry in the Antarctic stratospheric ozone depletion in September 1993: a) effect on the stratospheric vertical column, b) effect at 16 km altitude (~100 hPa) and c) averaged meridional slice at 0º longitude, in which the effect of iodine chemistry can be seen spatially as a function of latitude and altitude. The relative percentage difference has been computed as ((iodine run – no iodine run) / no iodine run) × 100.

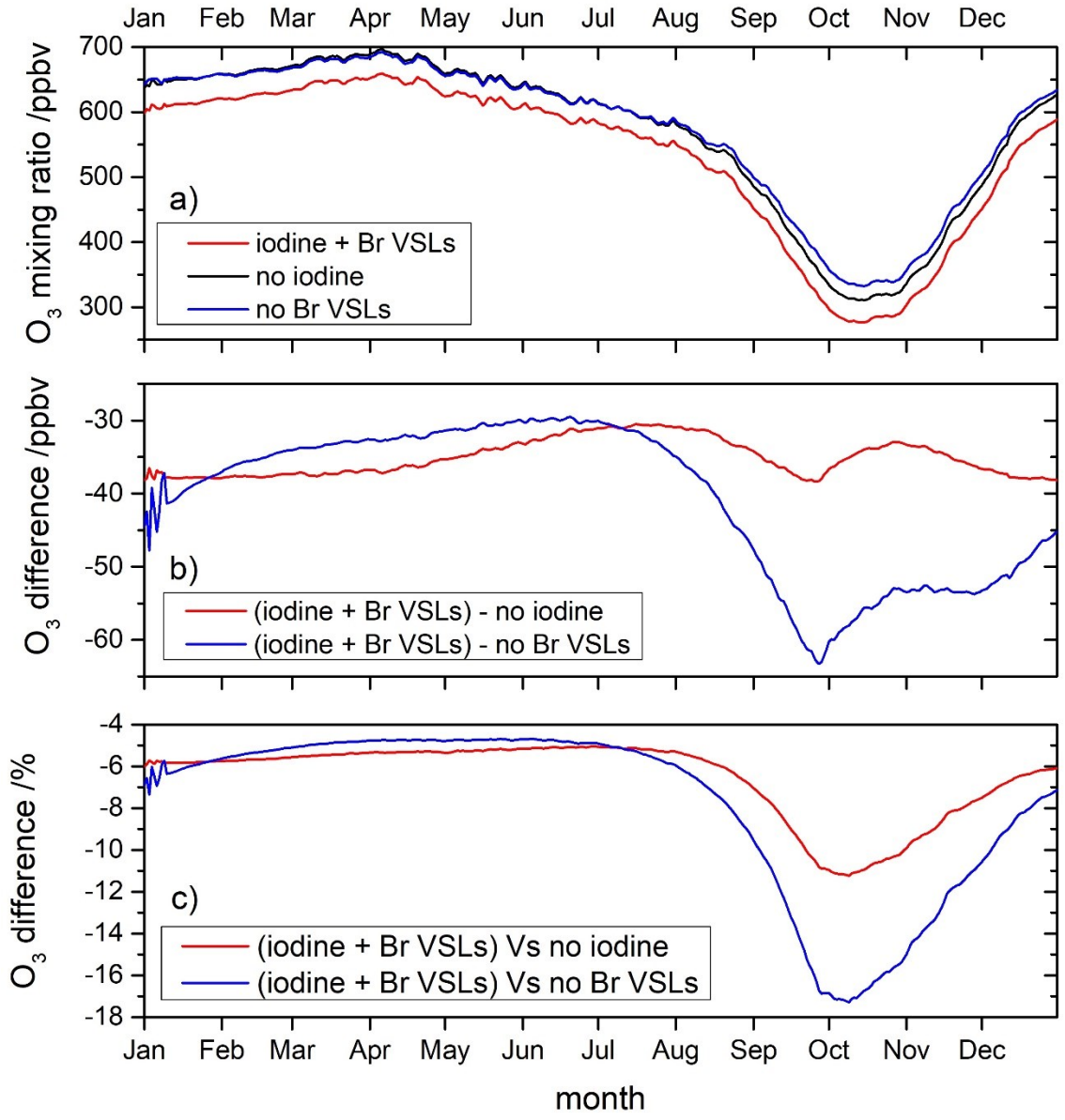

Figure S7. Daily evolution of the ozone hole during the 1980-2015 period in the region 90ºS-70ºS at 11-16 km altitude for the three simulations (a). The iodine run includes the three halogen chemical scheme (red line), the no iodine run includes only bromine and chlorine (black line), and the no Br VSLs run includes only iodine and chlorine VSLs (blue line). b) shows the ozone absolute difference in ppbv between the iodine and the no iodine runs and the difference between the iodine and no Br VSLs run. c) is the same as b) but displaying the ozone difference in percentage.

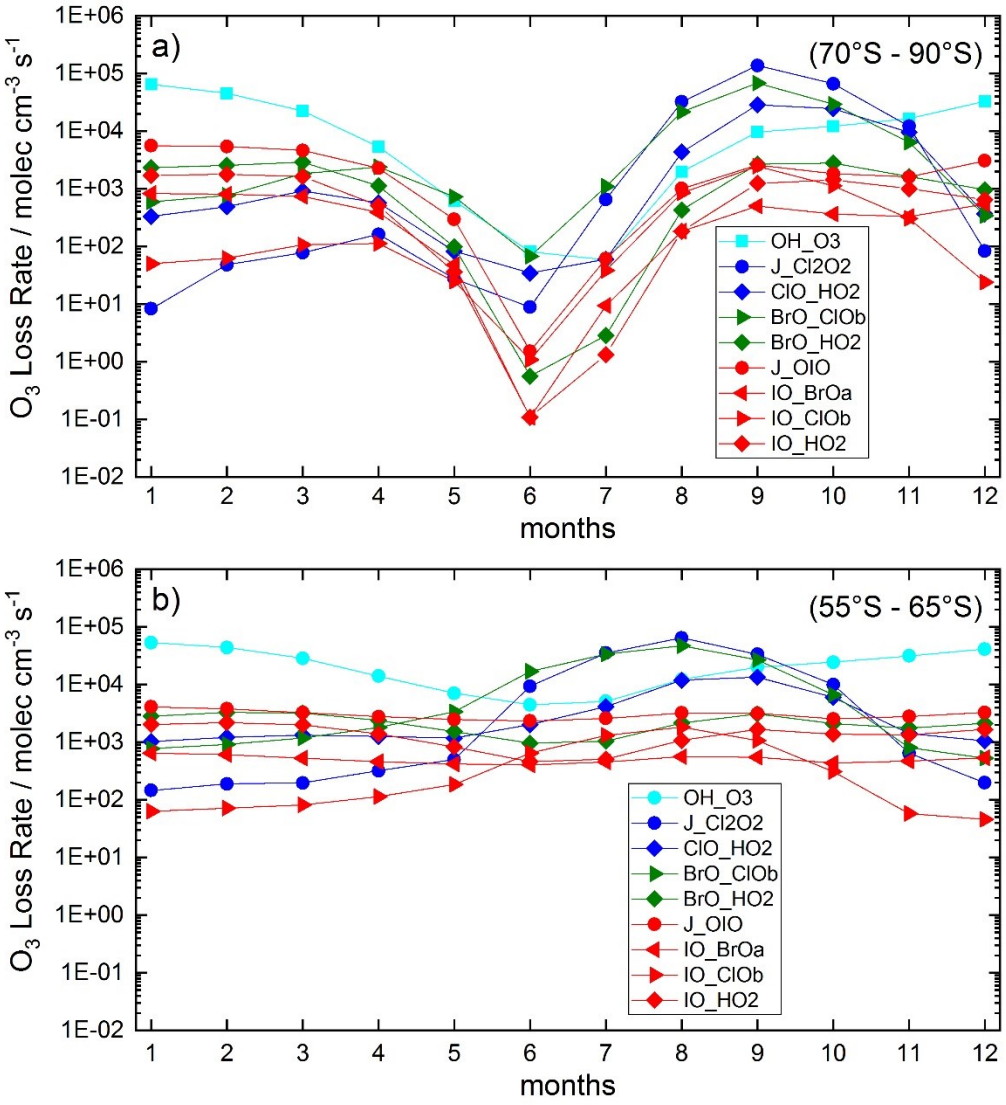

Figure S8: Absolute ozone loss rates averaged inside (90º-70ºS) and outside (55º-65ºS) the polar vortex at an altitude of 11-16 km (100 hPa). a) main loss rates for each family (grouped in colors) during spring for the simulation with iodine inside the polar vortex b) is the same as a) for mid-latitudes (65ºS-55ºS). J(OIO) is the main channel in both regions, although inside the polar vortex this channel is matched by IO_ClO during spring. Outside the polar vortex the second channel is IO_HO_2, followed by IO_BrO. Only during wintertime, the IO_ClO channels become more important but never exceed the J(OIO) channel.

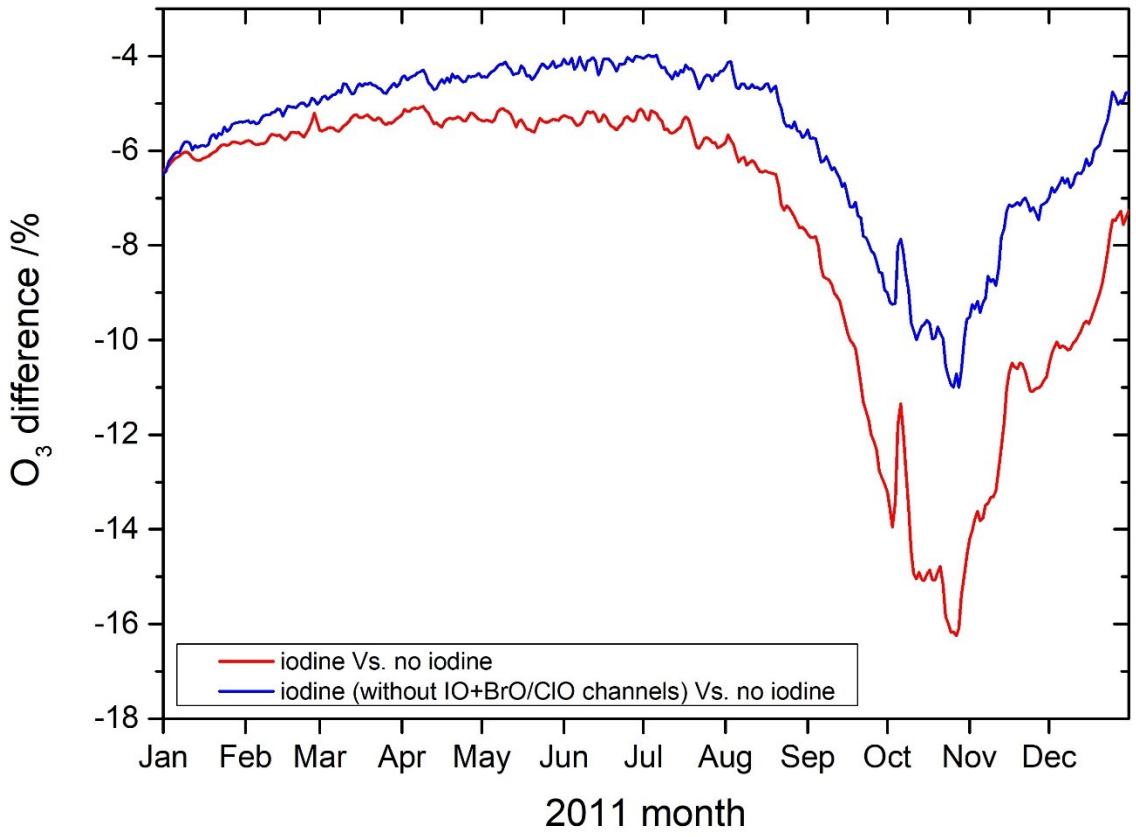

Figure S9. Relative daily evolution of ozone levels during 2011 in the region 90ºS-70ºS at 11-16 km altitude. The red line represents the ozone relative difference between the iodine run and the no iodine run, while the blue line is the ozone relative difference between the iodine run without the IO+BrO/ClO channels above the tropopause in the polar regions and the no iodine run. The standard iodine run destroys up to 16% at the end of October in 2011 compared to the no iodine run, while the iodine without the IO+BrO/ClO channels run destroys up to 11%. The 5 percentage points difference is the contribution from the IO+BrO/ClO channels in 2011 in the Antarctic spring.

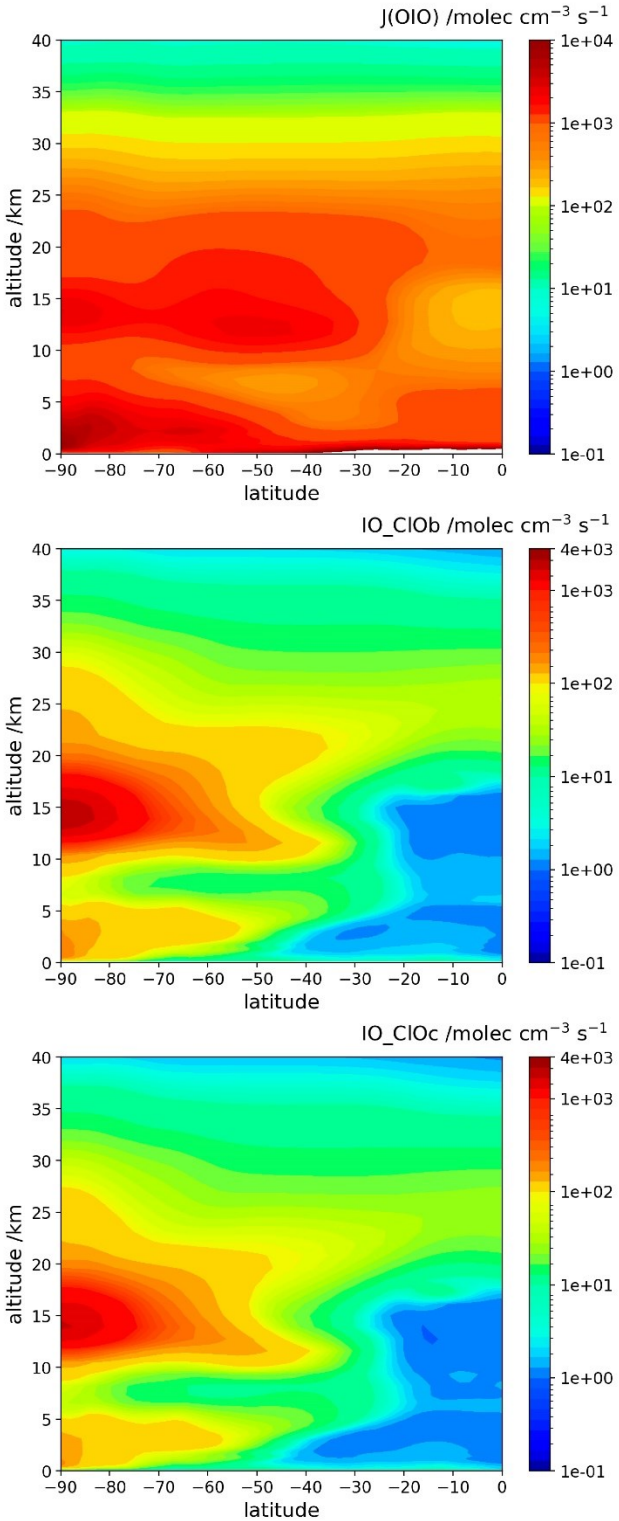

Figure S10. 1980-2015 October zonally averaged rates of the two main iodine channels [IO-ClO and J(OIO)] involved in ozone depletion in the Antarctic stratosphere. The highest rates are below 16 km altitude, where reactant concentrations and temperatures conditions enhance the reactions OIO + hv → I + O_2 [J(OIO)], IO + ClO → I + Cl + O_2 [IO_ClOb] and IO + ClO → ICl + O_2 [IO_ClOc]. OIO abundance in springtime is very small (Fig. S10a), given the very fast photo-dissociation, but

its distribution can be inferred from its main source species IO (IO+IO → OIO + I and IO+O_3 → OIO + O_2). Similarly, for the reactions of IO+ClO, ClO can be considered as kinetically being in excess with respect to IO, and the temperature and ozone levels more favourable for the formation of IO occurs at the 13-16 km altitude.

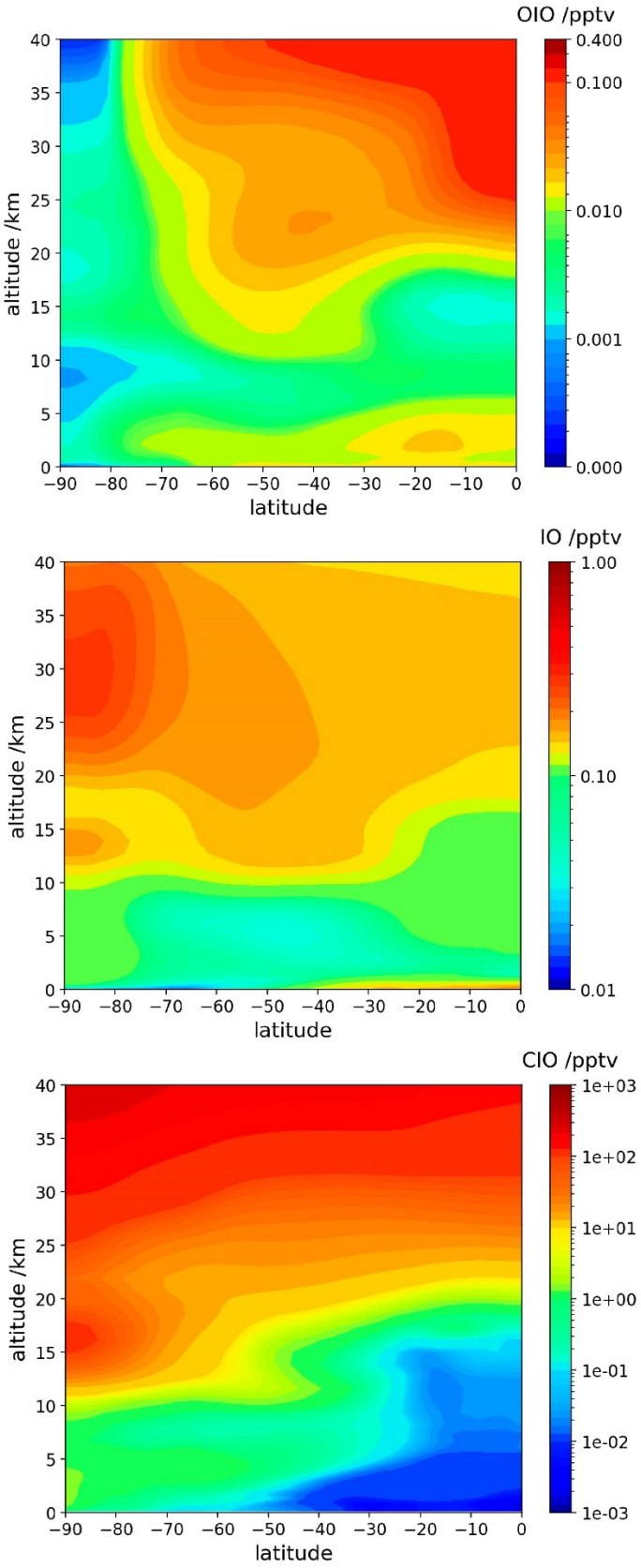

Figure S11. 1980-2015 October zonal averaged mixing ratios of OIO, IO and ClO.

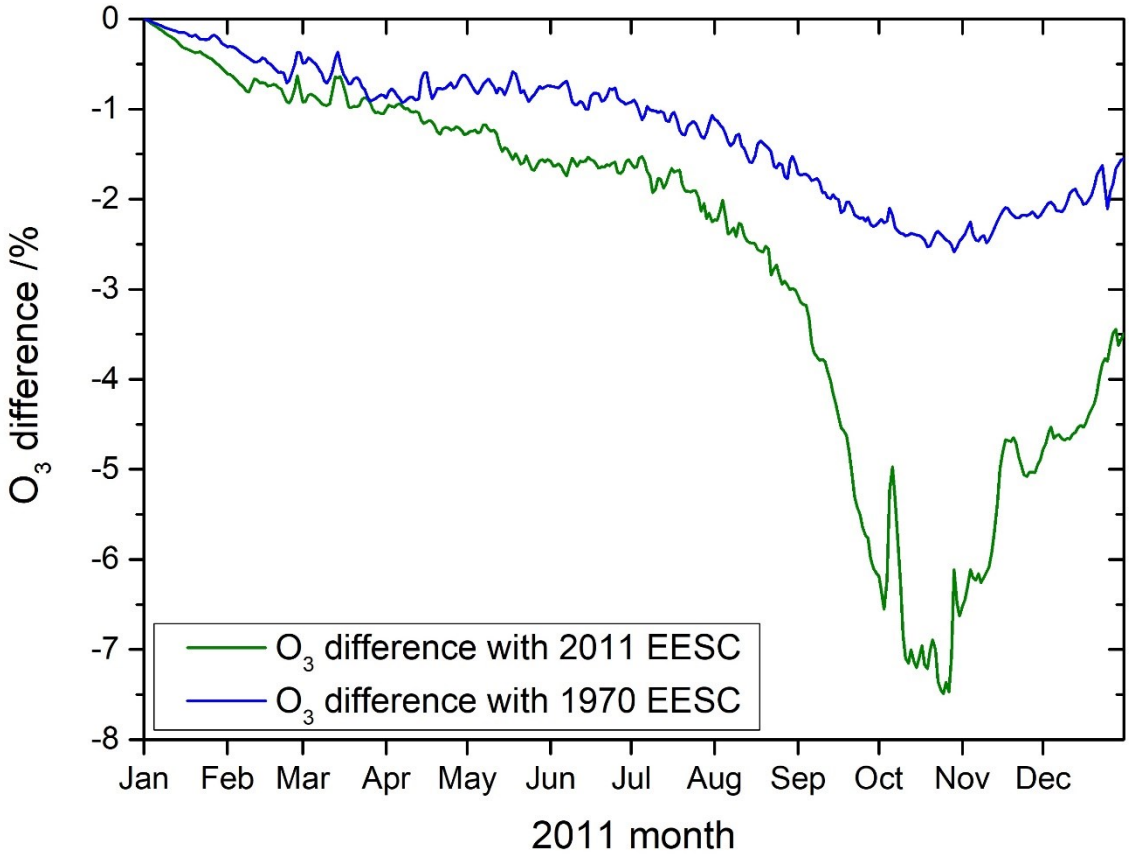

Figure S12. Daily evolution of the relative ozone difference in the region 90ºS-70ºS at 11-16 km altitude, for the different runs in the sensitivity performed making zero the values of the IO+ClO/BrO cross reaction channels above the tropopause during 2011, an also scaling chlorine and bromine levels to those in 1970. Both lines represent the ozone relative difference between the iodine run and the no iodine run with cross reaction rate constants zeroed (green line for 2011 EESC and blue line for 1970 EESC). In the September through October ozone hole period there is more depletion when cross reactions are included. E.g., October shows 8% and 2.5% more ozone when the cross reactions are zeroed for 2011 and 1970 EESC conditions (both EESC conditions use year 2011 met conditions). In October, there is three times more sensitivity of the cross reactions at higher (vs lower) EESC (i.e., 8/2.5 = 3.2). This sensitivity results, during the ozone period, show the coupled reaction sensitivity is impacted by the ClO_x/BrO_x abundance. More ClO_x and BrO_x in 2011 produces more depletion compared to 1970. So the with and without IO+ClO/BrO reactions are showing a 2.5% increase with 1970 conditions and 8.0% increase with 2011 conditions. The ratio of 8.0/2.5 is an indication of the sensitivity to the EESC.

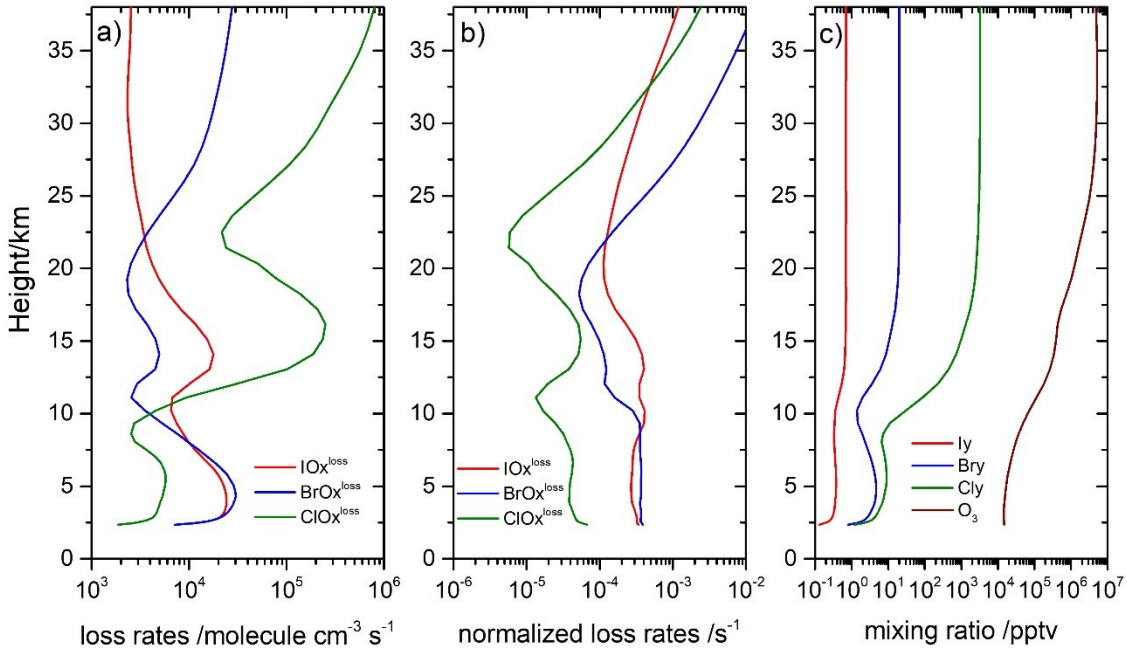

Figure S13. Absolute ozone loss rates for the three families $BrOx^{loss}$, $ClOx^{loss}$ and IOx^{loss} (a), ozone loss rates for the three halogen families normalized to Br_y, Cl_y and I_y concentrations (b), and vertical profile of I_y, Br_y and Cl_y and ozone (c). The data in this figure are results for mean October 1980-2015 output averaged in the 90ºS-70ºS region from the simulation with iodine. Note: in the middle panel, ozone loss rates for I_x have been normalized to I_y+Br_y mixing ratios.

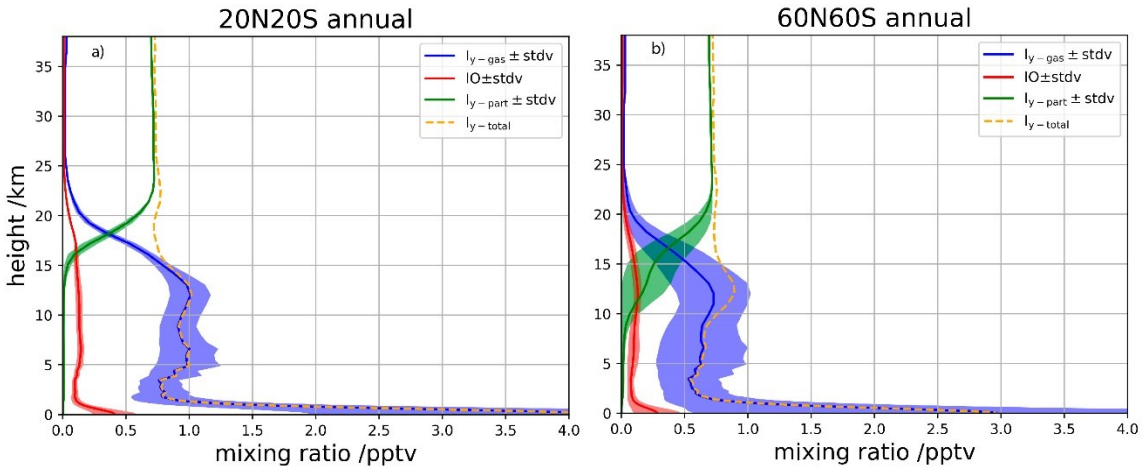

Figure S14. Present-day (2015) annual averaged vertical profile of modelled I_y the tropics (20ºS-20ºN) (a) and 60ºS-60ºN regions (b). Shaded areas represent the standard deviation ((±σ)). These modelled data from the "I_{part}" lower limit simulation include a fraction of reactive iodine in gas phase, and the rest as particulate iodine. The dash yellow line (the sum of $I_{y,gas}$ and I_{part}, or the equivalent to all iodine in gas phase) produces 10% reduction of stratospheric ozone in the lower part (90º-70ºS and 11-16 km altitude) of the Antarctic stratospheric ozone hole. While the blue line (the remaining I_y in gas phase in a simulation implementing particulate iodine) produces a 3.5% reduction.

	CASSCF/aug-cc-pVTZ		MRCI+Q/aug-cc-pVTZ	
	Ev(nm)	Ead (nm)	Ev(nm)	Ead (nm)
S0	--	--	--	
T1	285	516	**259**	**490***
T2	262		258	
S1	240	427	**225**	**442***
S2	239		220	

**Not corrected with ZPE*

Table S1: Adiabatic (E_{ad}) and vertical (Ev) excitation energies in nm

Ground state S_0 (MRCI/USERDEF ENERGY=-520.10916268)			
I	0.4255210134	-0.2373158700	-0.3727807612
O	-0.4151984781	1.2188623569	0.3242599813
O	2.1070035827	-0.2373158700	0.3242607988
O	-0.4151984781	-1.6934940969	0.3242599813
First excited state S1 (MRCI/USERDEF ENERGY=-520.00593233)			
I	0.4255204022	-0.2373158700	0.0434215365
O	-0.5313697158	1.4200706520	0.1855258269
O	2.3393466693	-0.2373158700	0.1855268097
O	-0.5313697157	-1.8947023919	0.1855258269
First triplet state T1 (MRCI/USERDEF ENERGY=-520.01590078)			
I	0.4255040992	-0.2373986019	0.1068690058
O	-0.4858157770	1.3412221630	0.1565547973
O	2.2482541634	-0.2372888314	0.1593931470
O	-0.4858148455	-1.8157982095	0.1631130500

Table S2: XYZ coordinates at MRCI+Q/aug-cc-pVTZ-PP

IO_3^-(CASSCF/aug-cc-pVTZ)							
	ω_1	ω_2	ω_3	ω_4	ω_5	ω_6	ZPE
S_0	795	795	748	326	278	278	1611
S_1	532	468	468	434	86	85	1038
S_2	1046	567	489	489	132	132	1428
T_1	552	504	504	256	31	31	908

Table S3: CASSCF/aug-cc-pVTZ harmonic vibrational frequencies (ω_i in cm^{-1}) of the low-lying electronic state of IO_3^-.

Reaction	Liquid binary and ternary sulphate polar stratospheric cloud particles reactions	Reactive uptake
R1	$N_2O_5 + H_2O(l) \rightarrow 2HNO_3$	γ=f(wt%)
R2	$ClONO_2 + H_2O(l) \rightarrow HOCl + HNO_3$	γ=f(T, P, HCl, H_2O ,r)
R3	$BrONO_2 + H_2O(l) \rightarrow HOBr + HNO_3$	γ=f(T, P, H_2O ,r)
R4	$ClONO_2 + HCl(l) \rightarrow Cl_2 + HNO_3$	γ=f(T, P, HCl, H_2O ,r)
R5	$HOCl + HCl(l) \rightarrow Cl_2 + H_2O$	γ=f(T, P, HCl, HOCl, H_2O ,r)
R6	$HOBr + HCl(l) \rightarrow BrCl + H_2O$	γ=f(T, P, HCl, HOBr, H_2O ,r)
R7	$HOCl + HBr(l) \rightarrow BrCl + H_2O$	γ=γ(R6)
R8	$HOBr + HBr(l) \rightarrow Br_2 + H_2O$	γ=γ(R6)
R9	$HOCl + HI(l) \rightarrow ICl + H_2O$	γ=γ(R6)
R10	$HOBr + HI(l) \rightarrow IBr + H_2O$	γ=γ(R6)
R11	$IONO_2 + H_2O(l) \rightarrow HOI + HNO_3$	γ=γ(R3)
R12	$HOI + HCl(l) \rightarrow ICl + H_2O$	γ=γ(R6)
R13	$HOI + HBr(l) \rightarrow IBr + H_2O$	γ=γ(R6)
R14	$HOI + HI(l) \rightarrow I_2 + H_2O$	γ=γ(R6)
R15	$IONO_2 + H_2O(l) \rightarrow I_{part}$	γ=0.01
R16	$HOI + HCl(l) \rightarrow I_{part}$	γ=0.01
	Nitric acid trihydrate reactions	
R17	$N_2O_5 + H_2O(s) \rightarrow 2HNO_3$	γ=0.0004, JPL10-6 (4)
R18	$ClONO_2 + H_2O(s) \rightarrow HOCl + HNO_3$	γ=0.004, JPL10-6 (4)
R19	$ClONO_2 + HCl(s) \rightarrow Cl_2 + HNO_3$	γ=0.2, JPL10-6 (4)
R20	$HOCl + HCl(s) \rightarrow Cl_2 + H_2O$	γ=0.1, JPL10-6 (4)
R21	$HOBr + HCl(s) \rightarrow BrCl + H_2O$	γ=γ(R20)
R22	$HOCl + HBr(s) \rightarrow BrCl + H_2O$	γ=γ(R20)
R23	$HOBr + HBr(s) \rightarrow Br_2 + H_2O$	γ=γ(R20)
R24	$HOCl + HI(s) \rightarrow ICl + H_2O$	γ=γ(R20)
R25	$HOBr + HI(s) \rightarrow IBr + H_2O$	γ=γ(R20)
R26	$BrONO_2 + H_2O(s) \rightarrow HOBr + HNO_3$	γ=0.006 Davies et al., 2002 (5)
R27	$IONO_2 + H_2O(s) \rightarrow HOI + HNO_3$	γ=γ(R26)
R28	$HOI + HCl(s) \rightarrow ICl + H_2O$	γ=γ(R20)
R29	$HOI + HBr(s) \rightarrow IBr + H_2O$	γ=γ(R20)
R30	$HOI + HI(s) \rightarrow I_2 + H_2O$	γ=γ(R20)
R31	$IONO_2 + H_2O(s) \rightarrow I_{part}$	γ=0.01
R32	$HOI + HCl(s) \rightarrow I_{part}$	γ=0.01
	Water ice polar stratospheric particles reactions	
R33	$N_2O_5 + H_2O(s) \rightarrow 2HNO_3$	γ=0.02, JPL10-6 (4)
R34	$ClONO_2 + H_2O(s) \rightarrow HOCl + HNO_3$	γ=0.3, JPL10-6 (4)
R35	$BrONO_2 + H_2O(s) \rightarrow HOBr + HNO_3$	γ=0.3, JPL10-6 (4)
R36	$ClONO_2 + HCl(s) \rightarrow Cl_2 + HNO_3$	γ=0.3, JPL10-6 (4)
R37	$HOCl + HCl(s) \rightarrow Cl_2 + H_2O$	γ=0.2, JPL10-6 (4)
R38	$HOBr + HCl(s) \rightarrow BrCl + H_2O$	γ=0.3, JPL10-6 (4)
R39	$HOCl + HBr(s) \rightarrow BrCl + H_2O$	γ=γ(R37)
R40	$HOBr + HBr(s) \rightarrow Br_2 + H_2O$	γ=γ(R38)
R41	$HOCl + HI(s) \rightarrow ICl + H_2O$	γ=γ(R37)
R42	$HOBr + HI(s) \rightarrow IBr + H_2O$	γ=γ(R37)
R43	$IONO_2 + H_2O(s) \rightarrow HOI + HNO_3$	γ=γ(R35)
R44	$HOI + HCl(s) \rightarrow ICl + H_2O$	γ=γ(R38)
R45	$HOI + HBr(s) \rightarrow IBr + H_2O$	γ=γ(R38)
R46	$HOI + HI(s) \rightarrow I_2 + H_2O$	γ=γ(R38)
R47	$IONO_2 + H_2O(s) \rightarrow I_{part}$	γ=0.01

R48	$HOI + HCl(s) \rightarrow I_{part}$	γ=0.01

Table S4. Summary of stratospheric heterogeneous bromine, chlorine and iodine reactions on liquid binary and ternary sulfate polar stratospheric cloud particles, nitric acid trihydrate and water ice polar stratospheric particles considered in WACCM4. Uptake coefficients (γ) for iodine reactions have been mapped to their equivalent reactions for bromine. Reactions highlighted in blue are the additional heterogeneous iodine reactions with respect to the standard WACCM scheme.

SI References

1. H. Wen, G.-L. Hou, W. Huang, N. Govind, X.-B. Wang, Photoelectron spectroscopy of higher bromine and iodine oxide anions: Electron affinities and electronic structures of BrO2,3 and IO2–4 radicals. *J. Chem. Phys.* **135**, 184309 (2011).

2. Ó. Gálvez, M. T. Baeza-Romero, M. Sanz, A. Saiz-Lopez, Photolysis of frozen iodate salts as a source of active iodine in the polar environment. *Atmos. Chem. Phys.* **16**, 12703–12713 (2016).

3. S. Tilmes, *et al.*, Technical Note: Ozonesonde climatology between 1995 and 2011: description, evaluation and applications. *Atmos. Chem. Phys.* **12**, 7475–7497 (2012).

4. JPL, Chemical Kinetics and Photochemical Data for Use in Atmospheric Studies, vol. 17. *JPL Publ. 10-6, Jet Propuls. Lab., Pasadena* (2011).

5. S. Davies, *et al.*, Modeling the effect of denitrification on Arctic ozone depletion during winter 1999/2000. *J. Geophys. Res. Atmos.* **107**, SOL 65-1-SOL 65-18 (2002).